

# Determination of $1p$ and $2p$ stripping excitation functions for $^{16}\text{O}+^{142}\text{Ce}$ using a Recoil Mass Spectrometer

Rohan Biswas<sup>a</sup>, S. Nath<sup>a,\*</sup>, J. Gehlot<sup>a</sup>, Gonika<sup>a</sup>, Chandra Kumar<sup>a</sup>, A. Parihari<sup>b</sup>, N. Madhavan<sup>a</sup>, A. Vinayak<sup>c</sup>, Amritraj Mahato<sup>d</sup>, Shoaib Noor<sup>e</sup>, Phurba Sherpa<sup>b</sup>, Kazuyuki Sekizawa<sup>f,g</sup>

<sup>a</sup>Nuclear Physics Group, Inter-University Accelerator Centre, Aruna Asaf Ali Marg, New Delhi 110067, India

<sup>b</sup>Department of Physics and Astrophysics, Delhi University, Delhi 110007, India

<sup>c</sup>Department of Physics, Karnatak University, Dharwad 580003, India

<sup>d</sup>Department of Physics, Central University of Jharkhand, Ranchi 835205, India

<sup>e</sup>School of Physics and Materials Science, Thapar Institute of Engineering and Technology, Patiala 147004, India

<sup>f</sup>Department of Physics, School of Science, Tokyo Institute of Technology, Tokyo 152-8551, Japan

<sup>g</sup>Nuclear Physics Division, Center for Computational Sciences, University of Tsukuba, Ibaraki 305-8577, Japan

arXiv:2109.03203v1 [nucl-ex] 7 Sep 2021

---

## Abstract

We report the first direct measurement of differential transfer cross sections using a Recoil Mass Spectrometer. Absolute differential  $1p$  and  $2p$ -stripping cross sections at  $\theta_{\text{c.m.}} = 180^\circ$  have been determined for the system  $^{16}\text{O}+^{142}\text{Ce}$  by detecting the heavier target-like ions at the focal plane of the Heavy Ion Reaction Analyzer. Focal plane spectra have been compared with the results of a semi-microscopic Monte-Carlo simulation to unambiguously identify the transfer channels. Transmission efficiency of the target-like ions through the spectrometer has also been estimated using the simulation which has been crucial to extract the cross sections from the yields of ions measured during the experiment. The methodology adopted in this work can be applied to measure multi-nucleon transfer cross sections using other similar recoil separators. The experimental excitation functions for the reactions  $^{142}\text{Ce}(^{16}\text{O},^{15}\text{N})^{143}\text{Pr}$  and  $^{142}\text{Ce}(^{16}\text{O},^{14}\text{C})^{144}\text{Nd}$  have been compared with coupled reaction channel calculations. An excellent matching between measurement and theory has been obtained. For  $1p$ -stripping, major contribution to the cross section has been found to be the transfer of a proton from  $^{16}\text{O}$  to the  $2d_{5/2}$  excited state of  $^{143}\text{Pr}$ , leaving behind  $^{15}\text{N}$  in the  $1p_{1/2}$  ground state. Transfer of a cluster of two protons from  $^{16}\text{O}$  to the  $2^+$  excited state of  $^{144}\text{Nd}$ , resulting in  $^{14}\text{C}$  in the  $0^+$  ground state, appears to be the most probable cause for  $2p$ -stripping. Measured transfer probabilities for  $1p$  and  $2p$  channels have been compared with Time-Dependent Hartree-Fock calculations. Proton stripping channels are found to be more favourable compared to neutron pick-up channels. However, the theory overpredicts the measurement hinting at the need for extended approaches with explicit treatment of pairing correlations in the calculations.

---

## 1. Introduction

The simplest picture of a nuclear reaction is a light projectile ion being scattered off a heavier target nucleus. Such a collision, termed as *direct nuclear reaction* is characterized by a very short interaction time  $\sim 10^{-22}$  s and active participation of a few nucleons. In contrast, a *compound nuclear reaction* is much slower in which all the constituent nucleons of the collision partners take part to form a mono-nucleus. The resulting ‘compound nucleus’ decays by emission of photons and evaporation of light particles. Availability of heavy ion beams made a third and intermediate class of nuclear reactions possible [1]. Such reactions are characterized by creation of binary products in the exit channels with broad mass, charge and angular distributions. Heavy ion-induced reactions, with features

intermediate between direct reactions and compound nuclear reactions, had been variously termed as deep inelastic collision (DIC), multi-nucleon transfer (MNT), deep-inelastic transfer, quasi-fission, strongly-damped collision and relaxation phenomena by different research groups [2].

MNT reactions have been useful for synthesizing nuclides away from the valley of  $\beta$ -stability [3]. A renewed interest in the study of MNT reactions have been ignited by favourable predictions of synthesis of neutron-rich isotopes of heavy elements [4, 5] in the recent past. Knowledge about properties of the nuclides in the ‘north-east’ corner of the nuclear chart, in the vicinity of  $N = 126$  shell, is very important for better understanding of stellar nucleosynthesis via the  $r$ -process. Transfer of nucleons is also known to influence the dynamics of fusion between two heavy nuclei [6, 7].

Products of MNT reactions had earlier been identified by chemical separation and measurement of characteristic  $\gamma$ -rays [8]. Magnetic spectrographs of varied configurations [9] had also been used to detect the scattered projectile-like

---

\*Corresponding author

Email addresses: subir@iuac.res.in (S. Nath), sekizawa@phys.titech.ac.jp (Kazuyuki Sekizawa)

ions from MNT reactions. In the last two decades, a new class of magnetic separators [10–12] with large acceptance, has been put to use in the study of MNT reactions [13–15]. Production of neutron-rich nuclides in damped collisions has been studied recently with novel applications of a few recoil separators which were not originally designed and built for this purpose [16–18]. Production of nuclei far from the stability region in multi-nucleon transfer reactions using a high resolution magnetic spectrometer has also been reported recently [19].

In MNT reactions, either the projectile-like or the target-like ions can be detected at the focal plane of the recoil separator [20]. In most separators, usually the lighter projectile-like ions are detected in the forward angles in the laboratory frame of reference. Mass and charge of the corresponding target-like ions can be deciphered from two-body collision kinematics. Conversely, the heavier target-like ions can also be detected at the forward angles. This technique was first successfully used in the measurement of sub-barrier transfer reactions for  $^{58}\text{Ni}+^A\text{Sn}$  [21, 22] using the Daresbury recoil mass separator [23]. Target-like nuclei, separated according to their mass ( $A$ ) to charge state ( $q$ ) ratio,  $\left(\frac{A}{q}\right)$ , were detected by a position-sensitive detector at the focal plane of the separator. Rehm [8] pointed out that such a device had very limited dynamic range in velocity and charge acceptances. However, the excellent mass resolution made them quite useful in studying MNT reactions. Similar method was adopted for measurement of MNT probability, especially at sub-barrier energies, using other recoil mass spectrometers (RMSs) [24–26]. The Heavy Ion Reaction Analyzer (HIRA) [27], the first generation RMS at IUAC, New Delhi had also been employed to measure few nucleon transfer probabilities in several medium-heavy systems [28–33]. All these measurements suffered from two major drawbacks. Firstly, while estimating the transfer probability, it had been assumed that the elastic channel and all the transfer channels had same efficiency for transmission to the focal plane detector. Secondly, differential transfer cross sections had not been extracted from the data in most cases, as the transmission efficiency ( $\epsilon$ ) of the RMS [34] had not been known. Differential  $1n$ - and  $2n$ -transfer cross sections had been extracted for a limited number of reactions [21, 22, 24] with the additional assumption that the sum of differential elastic, inelastic and transfer cross sections was equal to the differential Rutherford scattering cross section at energies near and below the Coulomb barrier. Biswas *et al.* recently reported a methodology [35, 36] to overcome these assumptions and *measure* differential quasi-elastic scattering cross sections in an RMS.

In this Letter, we report the first direct measurement of differential transfer cross sections using an RMS. Differential cross sections for the reactions  $^{142}\text{Ce}(^{16}\text{O}, ^{15}\text{N})^{143}\text{Pr}$  and  $^{142}\text{Ce}(^{16}\text{O}, ^{14}\text{C})^{144}\text{Nd}$  have been extracted from yields recorded in the experiment. Details of the experiment are narrated in Section 2. We present results of the experi-

ment in Section 3. Coupled Reaction Channel (CRC) and Time-Dependent Hartree-Fock (TDHF) calculations, are described in Sections 4 and 5, respectively. Finally, in Section 6, we summarize and conclude our work.

## 2. The experiment

The experiment has been performed in two runs with a pulsed beam of  $^{16}\text{O}$  ions, having a pulse separation of  $4\ \mu\text{s}$ , accelerated through the 15UD Pelletron accelerator at IUAC, New Delhi. Isotopically enriched  $^{142}\text{Ce}$  target foils of thickness  $\sim 121.7\ \mu\text{g}/\text{cm}^2$ , sandwiched between two layers ( $\sim 20\ \mu\text{g}/\text{cm}^2$  backing and  $\sim 5\ \mu\text{g}/\text{cm}^2$  capping) of graphite films have been used as the target [37]. The targets also contained  $\sim 8\%$  impurity of  $^{140}\text{Ce}$ , which had been verified experimentally [37]. Beam energy ( $E_{\text{lab}}$ ) has been varied between 57–69 MeV. Two solid state silicon detectors (SSSD), each with a circular aperture of 1 mm diameter, have been placed at  $\theta_{\text{lab}} = 15^\circ$  in the horizontal plane at a distance of 100 mm from the target. These detectors have been used as beam monitors during the experiment and for normalization of cross-sections. The HIRA has been kept at  $\theta_{\text{lab}} = 0^\circ$  with an opening aperture of 5 mSr, corresponding to an angular acceptance of  $2.2^\circ$ . A thin ( $\sim 10\ \mu\text{g}/\text{cm}^2$ ) graphite foil has been placed 10 cm downstream from the target to reset charge states of the reaction products to equilibrium distribution. A Multi-Wire Proportional Counter (MWPC) of dimensions 150 mm in  $x$  and 50 mm in  $y$  has been placed at the focal plane of the HIRA. Here,  $x - z$  and  $y - z$  denote the dispersive and the non-dispersive planes of the RMS, respectively, with  $z$  being direction of the beam. Target-like ions, originating from quasi-elastic reactions, have been detected at the focal plane of the HIRA, spatially separated according to their  $\frac{A}{q}$ . Energy loss ( $\Delta E$ ) information has been obtained from the cathode of the MWPC. A Time-to-Amplitude Converter (TAC) has been set up to measure time-of-flight (TOF) of the ions through the HIRA, in which the anode signal from the MWPC and the radio-frequency (0.25 MHz RF) signal used for beam pulsing have been the start and the stop pulses, respectively.

Fig. 1 shows the  $\Delta E$ -TOF spectrum of the events detected at the focal plane of the HIRA at  $E_{\text{lab}} = 63$  MeV. Target-like ions have been identified by their higher  $\Delta E$  and closely-related TOF. The  $x$ -TOF spectrum at the same  $E_{\text{lab}}$ , gated with these events, are shown in Fig. 2(a). The most intense group with  $\frac{A}{q} = \frac{142}{14}$  corresponds to elastically / inelastically scattered  $^{142}\text{Ce}$  ions. Another charge state group of target-like nuclei from the elastic / inelastic channel(s), marked with  $\frac{142}{15}$ , can be seen in the extreme left of the figure. It is important to note here that we can not differentiate the inelastic channel(s) from the elastic channel in our method of measurement. Origin of the group marked with  $\frac{140}{14}$  is ambiguous. These ions may arise from elastic / inelastic scattering between the projectile nuclei and nuclei of  $^{140}\text{Ce}$ , present as impurities in the target foil [37]. Probable pickup of two

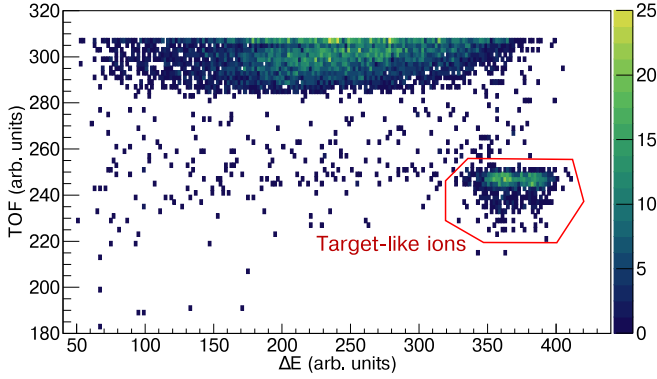


Figure 1: Scatter plot between  $\Delta E$  and TOF of the events recorded at the focal plane of the HIRA for  $^{16}\text{O}+^{142}\text{Ce}$  at  $E_{\text{lab}} = 63$  MeV. The target-like ions are marked.

neutrons from  $^{142}\text{Ce}$  ( $Q_0^{+2n} = -0.41$  MeV) may also lead to formation of  $^{140}\text{Ce}$ . Target-like ions, corresponding to probable  $1n$ -pickup ( $Q_0^{+1n} = -3.03$  MeV) channel, have not been identified as a distinct group in the  $\chi$ -TOF spectrum. The groups marked with  $\frac{143}{14}$  and  $\frac{144}{14}$  corresponding to  $1p$ - ( $Q_0^{-1p} = -6.303$  MeV) and  $2p$ -stripping ( $Q_0^{-2p} = -8.54$  MeV) channels, however, can be distinctly observed. While the recoiling target-like nuclei from  $1p$  channel ( $^{143}\text{Pr}$ ), have been recorded over the entire range of projectile energies, the same from  $2p$  channel, ( $^{144}\text{Nd}$ ), have been observed only at a few energies near the barrier, within the limited duration that have been available for collecting the data. It must be stated here that ascertaining the charge of the transferred nucleon(s) from the spectrum (Fig. 2(a)) alone is not possible. Identification of transfer channels have been realized with recourse to  $Q$ -value considerations.

Some residual background events, originating from multiple-scattering of projectile ions inside the spectrometer, can be observed in the measured  $\chi$ -TOF spectrum. Further rejection of background events can be achieved by making use of the method of kinematic coincidence between the recoiling target-like ions detected at the focal plane of the RMS and the back-scattered projectile-like ions detected by a  $\Delta E - E$  telescope [31].

### 3. Results

The elastic/inelastic and transfer channels in the experimental spectrum (Fig. 2(a)) have been identified based on their  $\frac{a}{q}$  values. To rule out any ambiguity in channel identification, the experimental spectrum has been further compared with a simulated  $\chi$ -TOF spectrum, which is shown in Fig. 2(b). The simulation has been carried out by a semi-microscopic Monte Carlo code [35, 36]. Simulated positions of the target-like ions, generated for the system  $^{16}\text{O}+^{142}\text{Ce}$ , *viz.*  $^{142}\text{Ce}$ , (elastic/inelastic)  $^{141}\text{Ce}$  ( $1n$ -pickup),  $^{140}\text{Ce}$  ( $2n$ -pickup),  $^{143}\text{Pr}$  ( $1p$ -stripping) and  $^{144}\text{Nd}$  ( $2p$ -stripping), are marked in Fig. 2(b). In addition, simulated positions of target-like ions which may result from collisions between  $^{16}\text{O}$  and  $^{140}\text{Ce}$  (impurity

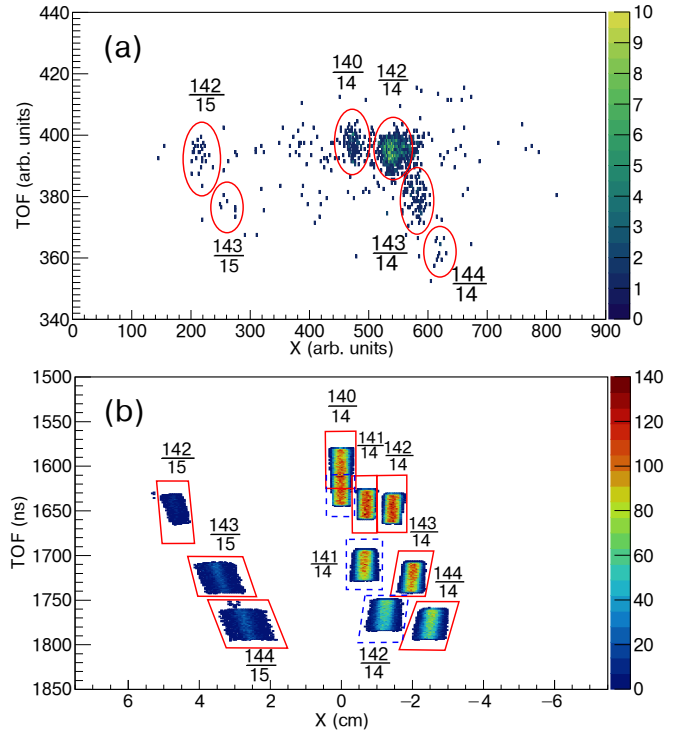


Figure 2: (a) Experimental and (b) simulated  $\chi$ -TOF spectra of target-like ions for the system  $^{16}\text{O}+^{142}\text{Ce}$  at  $E_{\text{lab}} = 63$  MeV. The identified channels are marked in panel (a). In panel (b), position of events from the elastic,  $1n$  and  $2n$  pick-up and  $1p$  and  $2p$  stripping channels for the system  $^{16}\text{O}+^{142}\text{Ce}$  are marked within boxes with solid (red) lines. Position of events from the elastic,  $1p$  and  $2p$  stripping channels for the system  $^{16}\text{O}+^{140}\text{Ce}$  are also shown in panel (b) and marked within boxes with dashed (blue) lines. See text for details.

in the target foil), *viz.*  $^{140}\text{Ce}$  (elastic/inelastic),  $^{141}\text{Pr}$  ( $1p$ -stripping) and  $^{142}\text{Nd}$  ( $2p$ -stripping), are also marked in the figure. Comparing the two panels of Fig. 2, we may conclude that (i) the target-like ions resulting from  $1n$ -pickup in the system  $^{16}\text{O}+^{142}\text{Ce}$  (marked  $\frac{141}{14}$  in the top half of panel (b)) can be distinguished from the elastic/inelastic products, if produced in the experiment, (ii) the two probable source of the group with  $\frac{a}{q} = \frac{140}{14}$  can not be resolved in TOF, (iii) the identification of  $1p$ - and  $2p$ -stripping channels for the system  $^{16}\text{O}+^{142}\text{Ce}$  is unambiguous and (iv) the target-like ions resulting from  $1p$ - and  $2p$ -stripping in the system  $^{16}\text{O}+^{140}\text{Ce}$  (marked  $\frac{141}{14}$  and  $\frac{142}{14}$  in the bottom half of panel (b)) should be identifiable, if produced in the experiment. This comparison underlines the need for highly-enriched isotopic target foils for such studies with RMS.

The absolute differential cross-sections for  $1p$  and  $2p$ -stripping at centre of mass (c.m.) angle,  $\theta_{\text{c.m.}} = 180^\circ$  have been calculated using the relation [36]:

$$\left(\frac{d\sigma}{d\Omega}\right)_{180^\circ}^{1p(2p)} = \frac{Y_{143(144)}}{Y_{\text{norm}}^{\text{Ruth}}} \frac{\Omega_{\text{norm}}}{\Omega_{\text{HIRA}}^{\text{eff}}} \frac{1}{\epsilon_{\text{HIRA}}} \left(\frac{d\sigma}{d\Omega}\right)_{\theta_{\text{norm}}}^{\text{Ruth}} \quad (1)$$

where  $Y_{143(144)}$  is the yield of the  $\frac{143}{q}$  ( $\frac{144}{q}$ ) group(s) in the  $\chi$ -TOF spectrum (Fig. 2) corresponding to  $1p$ -stripping ( $2p$ -stripping).  $Y_{\text{norm}}^{\text{Ruth}}$  is the geometric mean of the counts recorded in the two normalization detectors.  $\Omega_{\text{norm}}$  and  $(\frac{d\sigma}{d\Omega})_{\theta_{\text{norm}}}^{\text{Ruth}}$  are the solid angle subtended by each of the normalization detectors and the differential Rutherford scattering cross section in the c.m. frame of reference at  $\theta_{\text{norm}} = 16.32^\circ$  (corresponding to  $\theta_{\text{lab}} = 15^\circ$ ), respectively. The transmission efficiency  $\epsilon_{\text{HIRA}}$  for the target-like ions have been calculated [35] by taking the ratio of the counts of ions reaching the focal plane to the number of ions entering the entrance aperture of the HIRA. The effective solid angle,  $\Omega_{\text{HIRA}}^{\text{eff}}$ , has been determined experimentally by recording the target-like ions at  $E_{\text{lab}} = 48$  MeV using the relation [36]:

$$\Omega_{\text{HIRA}}^{\text{eff}} = \frac{Y_{142}^{\text{Ruth}}}{Y_{\text{norm}}^{\text{Ruth}}} \Omega_{\text{norm}} \frac{1}{\epsilon_{\text{HIRA}}} \left( \frac{d\sigma}{d\Omega} \right)_{\theta_{\text{norm}}}^{\text{Ruth}} / \left( \frac{d\sigma}{d\Omega} \right)_{180^\circ}^{\text{Ruth}}. \quad (2)$$

At this energy ( $\simeq 25\%$  below the Coulomb barrier), all scattering events obey Rutherford scattering and the transfer channels are closed. The absolute differential cross sections for  $1p$  and  $2p$  stripping channels, as a function of

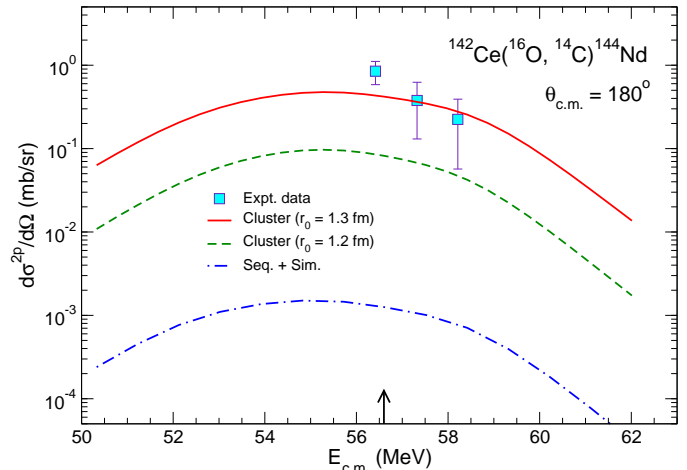


Figure 4: Absolute differential cross sections for the reaction  $^{142}\text{Ce}(^{16}\text{O}, ^{14}\text{C})^{144}\text{Nd}$  at  $\theta_{\text{c.m.}} = 180^\circ$  as a function of  $E_{\text{c.m.}}$ . Results of the combined sequential and microscopic simultaneous CRC calculations are shown by the dot-dashed (blue) line. Results of the extreme cluster model CRC calculations are shown by solid (red) line ( $r_0 = 1.3$  fm) and dashed (green) lines ( $r_0 = 1.2$  fm). The arrow denotes location of the Coulomb barrier.

Table 1: Systematic errors considered while extracting the experimental differential  $1p$  and  $2p$ -stripping cross-sections.

Quantity	Uncertainty	% effect
$\theta_{\text{norm}}$	$0.5^\circ$	$12.8^{\text{a}}$
$\Omega_{\text{norm}}$	$2.0$ mm <sup>b</sup>	$4.0$
$\epsilon_{\text{HIRA}}$	$10.0$ %	$10.0$
$\Omega_{\text{HIRA}}^{\text{eff}}$	$17.1$ %	$17.1$

<sup>a</sup> Error in calculated  $(\frac{d\sigma}{d\Omega})_{\theta_{\text{norm}}}^{\text{Ruth}}$

<sup>b</sup> Uncertainty in distance between target and detector

<sup>c</sup> Uncertainty in aperture diameter

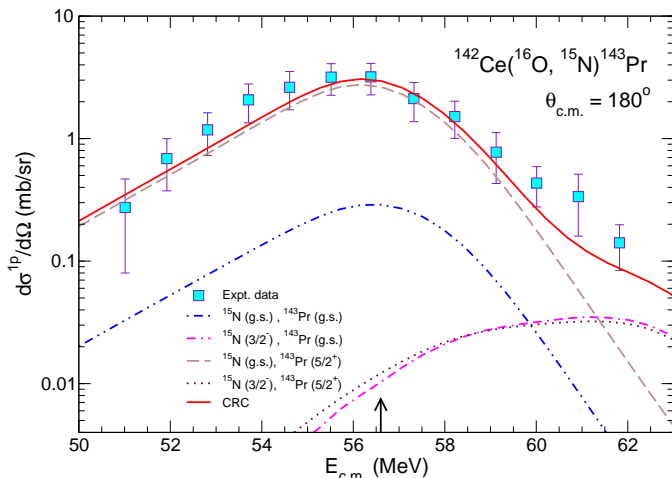


Figure 3: Absolute differential cross sections for the reaction  $^{142}\text{Ce}(^{16}\text{O}, ^{15}\text{N})^{143}\text{Pr}$  at  $\theta_{\text{c.m.}} = 180^\circ$  as a function of  $E_{\text{c.m.}}$ . The full CRC calculation is shown by the solid (red) line. Contributions of different exit channels to the transfer cross sections are also shown. The arrow denotes location of the Coulomb barrier.

Error bars in Fig. 3 and Fig. 4 include statistical as well as systematic uncertainties, the latter of which are listed in Table 1. The error in  $\Omega_{\text{HIRA}}^{\text{eff}}$  contains statistical uncertainties in the measured yields ( $Y_{142}^{\text{Ruth}}$  and  $Y_{\text{norm}}^{\text{Ruth}}$ ) at  $E_{\text{lab}} = 48$  MeV and similar systematic uncertainties.

#### 4. Coupled Reaction Channel calculations

Measured differential cross sections have been compared with finite-range CRC model calculations performed

using the code FRESKO [38, 39]. The coupling scheme is shown in Fig. 5. Reduced transition probability ( $B(E2)$ ) for transition to the  $2^+$  state of  $^{142}\text{Ce}$  has been taken to be  $4572$  e $^2\text{fm}^4$  [40]. Entrance channel, exit channel and core-core ( $^{15}\text{N}+^{142}\text{Ce}$ ) interactions for  $1p$ -stripping channel have been defined by optical potential containing real and imaginary parts, taken in Woods-Saxon shape where the parameters have been determined using Akyüz-Winther formalism [41]. The parameters of the optical potential, used in the calculations, are listed in Table 2. The real parameters have been determined at  $E_{\text{lab}} = 63$  MeV. Parameters of the imaginary part of the entrance channel optical potential have been determined by reproducing the elastic/inelastic scattering excitation function. The Woods-Saxon parameters for the proton bound-state potential in  $^{16}\text{O}$  have been taken from Ref. [42]. Global parameters [43] have been used to define the proton bound-state potential in  $^{143}\text{Pr}$ . Depth of the real part of bound-state potentials has been varied to reproduce the binding energy of the proton to the core. Spectroscopic factors for

the  $1p_{\frac{1}{2}}$  ground state (g.s.) and  $1p_{\frac{3}{2}}$  third excited state of  $^{15}\text{N}$  have been taken to be 1.275 and 2.047, respectively [42]. Spectroscopic factors for the overlaps between states in the target-like nuclei have been taken to be 1.0. The calculations have been performed in prior representation including full complex remnant terms.

Results of CRC calculations agree very well with the experimental cross sections for  $1p$  stripping, as shown in Fig. 3. The major contribution to the cross-sections is by the proton transfer to the  $2d_{\frac{5}{2}}$  state of  $^{143}\text{Pr}$  and g.s. to g.s. transfer between  $^{16}\text{O}$  and  $^{15}\text{N}$ . The hole state  $1p_{\frac{3}{2}}$  in  $^{15}\text{N}$ , which is at much higher excitation energy than the target-like nuclei, contribute to the cross sections at higher projectile energies.

To understand the mechanism for  $2p$  transfer in the reaction  $^{142}\text{Ce}(^{16}\text{O}, ^{14}\text{C})^{144}\text{Nd}$ , CRC calculations have been performed considering (a) combination of sequential (two-step) and microscopic simultaneous (one-step) processes and (b) extreme cluster model. Couplings considered in the sequential and microscopic simultaneous processes are shown in Fig. 5. The excited states in the intermediate nuclei have been taken to be the same as that for  $1p$  transfer. Global optical model parameters for the  $^{14}\text{C}+^{144}\text{Nd}$  exit channel and  $^{14}\text{C}+^{143}\text{Pr}$  core-core interaction are given in Table 2. The one-proton binding potential has been determined using the global optical model potential [43] where the depth of the real part has been adjusted to reproduce the one-proton binding energies to the  $^{14}\text{C}$  and  $^{143}\text{Pr}$  cores. Spectroscopic amplitudes of 0.9141 and 0.2867, respectively, have been used for the overlaps  $\langle ^{15}\text{N}(\frac{1}{2}^-) | ^{14}\text{C}(0^+) \rangle$

and  $\langle ^{15}\text{N}(\frac{3}{2}^-) | ^{14}\text{C}(0^+) \rangle$  [44]. Spectroscopic amplitudes for overlaps between  $^{143}\text{Pr}$  and  $^{144}\text{Nd}$  have been considered to be 1. The calculations have been done in prior-post combination to avoid the non-orthogonality terms. The same interaction potentials have been used in the microscopic simultaneous transfer process. The ground state ( $\psi_{\text{g.s.}}$ ) of  $^{16}\text{O}$  has been taken as [44]:

$$\psi_{\text{g.s.}} = 0.914 \left(1p_{\frac{1}{2}}\right)^2 + 0.405 \left(1p_{\frac{3}{2}}\right)^2$$

In this case, depth of the binding potential has been adjusted to reproduce half the  $2p$  separation energies. The calculations have been performed in prior form. In both the above methods, full complex remnant terms have been included in the calculations. The combined calculation underpredicts the experimental data by three orders of magnitude, as shown in Fig. 4. There is a minor increase in the cross sections (not shown in the figure) when the radius of binding potential well is changed to 1.3 fm. However, the increase remains insignificant with respect to the data.

In the extreme cluster model [46] analysis, the  $2p$  pair is considered to be anti-symmetric to each other with  $S = 0$  and  $T = 0$ . In the harmonic oscillator potential, the principle quantum number and orbital angular momentum parameters corresponding to individual protons ( $n_i, \ell_i$ ;  $i = 1, 2$ ) are transformed into  $(n, \ell)$  and  $(N, L)$ , corresponding to parameters relative to each other and to the c.m. of the core-cluster system, respectively. They are related through energy conservation by [47]:

$$\sum_{i=1,2} 2n_i + \ell_i = 2N + L + 2n + \ell \quad (3)$$

Assuming the proton pair to be in  $1s$  state ( $n = 1, \ell = 0$ ) relative to each other, we can find the combination of  $(N, L)$  using Eq. (3) to define the transfer of angular momentum according to the overlaps taken in Fig. 5. The CRC calculations have been performed by assigning  $(N = 2, L = 0)$  for  $\langle 0^+ | 0^+ \rangle$  transfer between  $^{16}\text{O}$  and  $^{14}\text{C}$ . For transfer between  $^{142}\text{Ce}$  and  $^{144}\text{Nd}$ , CRC calculations have been carried out for  $(N = 5, L = 0)$  for  $\langle 0^+ | 0^+ \rangle$ ,  $\langle 2^+ | 2^+ \rangle$  transfers and  $(N = 4, L = 2)$  for  $\langle 0^+ | 2^+ \rangle$ ,  $\langle 2^+ | 0^+ \rangle$  transfers. The two-proton Woods-Saxon binding potential well has been defined by radius  $r_0 = 1.2$  fm and diffuseness parameter  $a = 0.6$  fm [45], while depth of the potential has been adjusted to reproduce the  $2p$  separation energies. Spectroscopic amplitudes have been taken to be 1. The calculations have been performed in prior-form in which full complex remnant terms have been included. As observed in Fig. 4, the shape of the excitation function is the same as that for the sequential plus microscopic simultaneous calculations but the magnitude is larger by two orders. Yet, the calculations underpredict the data by an order. As the magnitude depends on the shape of the binding potential well [45], increasing the radius parameter to  $r_0 = 1.3$  fm has resulted in enhancement of the theoretical cross-sections by an order thus reproducing the experimental excitation function.

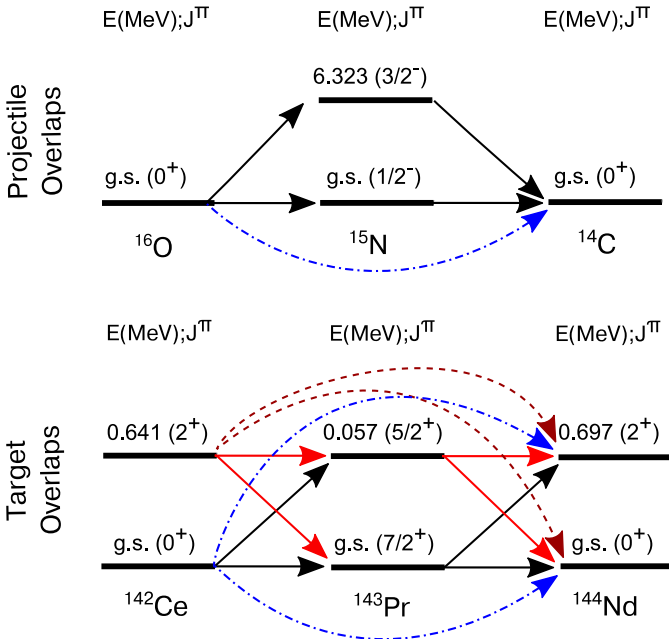


Figure 5: Coupling scheme adopted for CRC calculations of  $1p$  (solid arrows) and  $2p$  (dash-dotted arrows for g.s. of entrance channel and dashed arrows for excited state of entrance channel) transfer.

Table 2: Optical potential parameters used to define interaction between different channels. Depth ( $V_0$ ) of the real part of the potential is taken at  $E_{\text{lab}} = 63$  MeV.

System	$V_0$ (MeV)	$r_0$ (fm)	$a_0$ (fm)	$W_0$ (MeV)	$r_w$ (fm)	$a_w$ (fm)
$^{16}\text{O}+^{142}\text{Ce}$	61.859	1.2	0.651	50.0	1.0	0.4
$^{15}\text{N}+^{143}\text{Pr}$	59.571	1.2	0.647	14.893	1.0	0.4
$^{15}\text{N}+^{142}\text{Ce}$	59.387	1.2	0.649	14.847	1.2	0.649
$^{14}\text{C}+^{144}\text{Nd}$	57.070	1.2	0.647	14.267	1.2	0.647
$^{14}\text{C}+^{143}\text{Pr}$	56.893	1.2	0.647	14.223	1.2	0.647
$^{14}\text{C}+^{142}\text{Ce}$	56.714	1.2	0.647	14.178	1.2	0.647

No arbitrary normalization has been included in any of the calculated excitation functions.

## 5. Time-Dependent Hartree-Fock calculations

We have also analyzed the  $^{16}\text{O}+^{142}\text{Ce}$  reaction based on the microscopic framework of the Time-Dependent Hartree-Fock (TDHF) theory. A three-dimensional (3D) parallel TDHF code has been used, which has been continuously developed and applied for a variety of systems (see Ref. [48] and references therein), including various extensions going beyond the standard TDHF approach [49–52]. Here we provide information relevant to the present analysis. (For details of the theoretical framework and various applications, see, e.g., recent reviews [48, 53, 54].)

For the energy density functional (EDF), Skyrme SLy4d parameter set [55] has been used, which does not involve the c.m. correction in its fitting protocol [56]. Single-particle wave functions are represented by discretizing 3D Cartesian coordinates into a uniform grid with 0.8 fm grid spacing. For static Hartree-Fock calculations, a box of  $24^3 \text{ fm}^3$  has been used, while a box of  $64 \times 32 \times 24 \text{ fm}^3$  has been used for time-dependent simulations. The ground states of doubly-magic  $^{16}\text{O}$  is of spherical shape. Since the number of neutrons in  $^{142}\text{Ce}_{84}$  is close to the  $N = 82$  magic number, we have found that it is nearly of spherical shape in its Hartree-Fock ground state (with a tiny octupole deformation). We set the incident direction and the impact parameter ( $b$ ) vector parallel to the  $-x$  and  $+y$  directions, respectively, assigning  $x - y$  plane as the reaction plane. Since the deformation of the target nucleus ( $\beta_2 = 0.1259$ ) is small, we consider a single initial orientation of  $^{142}\text{Ce}$ , where a non-axial quadrupole moment,  $Q_{22} \propto \langle x^2 - y^2 \rangle$ , takes the smallest value in the reaction plane.

Once the EDF is fixed, the TDHF approach does not have adjustable parameters on reaction dynamics. In this sense, TDHF provides a non-empirical description of low-energy heavy-ion reactions. However, it is of course not a perfect framework since, e.g., it misses pairing correlations and mean-field fluctuations. Apart from the uncertainty inherent in the choice of an EDF, disagreements between TDHF and measurements could indicate importance of the physics beyond the TDHF approach. Keeping these points in mind, we compare the TDHF results with the experimental data for the  $^{16}\text{O}+^{142}\text{Ce}$  reaction.

Since the measurement has been carried out at  $\theta_{\text{c.m.}} = 180^\circ$ , TDHF calculations have been performed for head-on collisions (*i.e.*,  $b = 0$ ) between  $^{16}\text{O}$  and  $^{142}\text{Ce}$ , with changing collision energies. One should note that the relative motion of colliding nuclei (mean fields) is classical in TDHF. Hence, one can observe either fusion or non-fusion (not a superposition of them) depending on the initial conditions. For the present reaction at  $b = 0$ , we have found that  $E_{\text{c.m.}} \leq 56.6$  MeV results in binary reactions, whereas fusion takes place for  $E_{\text{c.m.}} \geq 56.7$  MeV.

For the binary reactions, we find that transfer of protons is more favorable than that of neutrons, although the absolute values are small. For instance, the average number of transferred protons reaches about 0.86 at the maximum for  $E_{\text{c.m.}} = 56.6$  MeV, while that of neutrons is rather small, less than 0.06 at the maximum. From a TDHF wave function after collision, one can extract transfer probabilities using the particle-number projection technique [57]. The extracted probabilities for quasi-elastic [(0p, 0n), without nucleon transfer], one-proton stripping ( $-1p$ ) and two-proton stripping ( $-2p$ ) reactions are shown in Fig. 6 as a function of the distance of the closest approach. The same is defined as

$$D = \frac{Z_p Z_t e^2}{2E_{\text{c.m.}}} \left( 1 + \text{cosec} \frac{\theta_{\text{c.m.}}}{2} \right), \quad (4)$$

where  $Z_p$  and  $Z_t$  are the atomic number of the projectile and the target, respectively,  $\theta_{\text{c.m.}}$  is the angle of the projectile-like ions in the c.m. frame of reference and  $e^2 = 1.44$  MeV fm. We note that one can obtain  $D$  from TDHF time evolution, which gives smaller values especially close to the fusion threshold. However, here we use Eq.4 for comparison with the experimental data.

As is apparent from Fig. 6, processes are dominated by the quasi-elastic scattering without nucleon transfer *i.e.* (0p, 0n) in the sub-barrier regime. Because of quantum tunneling of single-particle wave functions, there are small, yet finite probabilities for  $1p$  and  $2p$  stripping processes. The transfer probabilities increase with increasing  $E_{\text{c.m.}}$ , since it in turn decreases  $D$ . At energy close to the fusion threshold, probabilities of multi-nucleon transfer increase in TDHF as the system develop neck structure, although such behavior is not seen in the experimental data at  $E_{\text{c.m.}} \simeq 56.7$  MeV ( $D \simeq 11.8$  fm). From the figure, we find that TDHF systematically overestimates the transfer probability for  $1p$  stripping (about three times larger) as

compared to the measurements. The experimental data indicates that channels accompanying transfers of more than one proton are more probable than the TDHF prediction. However, experimental data for multi-proton transfer are not available in the sub-barrier regime. It is worth mentioning here that total kinetic energy loss (TKEL) is found to be at most 7 MeV for  $E_{c.m.} = 56.6$  MeV within the TDHF approach. Thus, particle evaporation effects are expected to be negligible in the sub-barrier region. It would be interesting to re-examine this reaction employing extended approaches that treat explicitly pairing correlations [58–63]. We note that the above-mentioned observation is consistent with the CRC analysis, *i.e.*, there is a

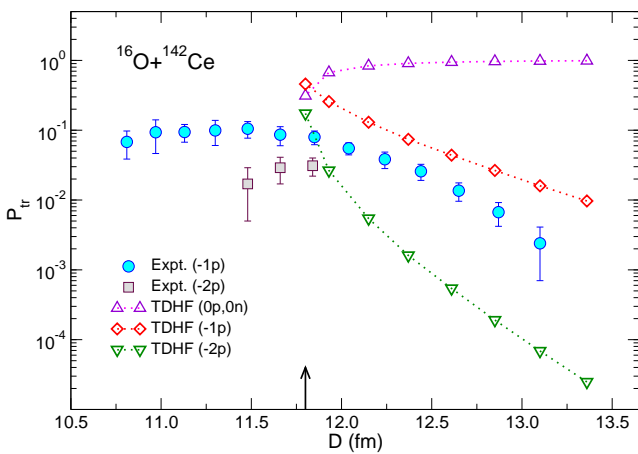


Figure 6: Transfer probabilities in the  $^{16}\text{O}+^{142}\text{Ce}$  reaction as a function of  $D$ . Experimental data for  $1p$  and  $2p$  stripping channels are shown by solid symbols. Results of TDHF calculations for quasielastic  $(0p,0n)$ ,  $(-1p)$ , and  $(-2p)$  channels are shown by open symbols, connected with dotted lines.

## 6. Conclusions

We demonstrate a novel method to measure multi-nucleon differential transfer cross sections directly, using an RMS, for the first time. Excitation functions for the reactions  $^{142}\text{Ce}(^{16}\text{O}, ^{15}\text{N})^{143}\text{Pr}$  and  $^{142}\text{Ce}(^{16}\text{O}, ^{14}\text{C})^{144}\text{Nd}$  have been measured around the Coulomb barrier. The heavier target-like ions have been detected at the focal plane of the HIRA, where ions from different exit channels are dispersed according to their  $\frac{A}{q}$  values. Information of  $\Delta E$  and TOF has further helped to reduce the background caused by randomly-scattered projectile-like ions. Ion trajectories inside the RMS have been simulated by a Monte-Carlo code to calculate the transmission efficiency of the target-like ions. The channels have been unambiguously identified with the aid of a comparison between the measured and simulated  $\chi$ -TOF spectra. This methodology can be adopted for measuring differential quasi-elastic cross sections in other similar recoil separators. CRC cal-

culations have been performed to understand the mechanism of  $1p$  and  $2p$  stripping. Transfer of a proton from  $^{16}\text{O}$  to the  $2d_{5/2}$  excited state of  $^{143}\text{Pr}$ , while  $^{15}\text{N}$  is left in the g.s., largely contributes to  $1p$ -stripping cross sections. At higher excitation energies, contribution from the  $1p_{3/2}$  hole state of  $^{15}\text{N}$  is found to be significant. Transfer of a cluster of two protons from the g.s. of  $^{16}\text{O}$  to the  $2^+$  excited state of  $^{144}\text{Nd}$ , with  $^{14}\text{C}$  remaining in the  $0^+$  g.s., best reproduces the  $2p$ -stripping cross sections. This observation is similar to other studies involving two-nucleon transfer [45, 64]. TDHF calculations indicate that proton(s) transfer is favoured compared to transfer of neutron(s) in the present reaction. We have found that TDHF calculations overpredict measured transfer probabilities, indicating that simultaneous transfer of two protons has a significant contribution. For better understanding, it is necessary to use extended approaches in which pairing correlations are explicitly taken into account.

## Acknowledgements

R.B. acknowledges Council of Scientific and Industrial Research (CSIR), New Delhi for financial support via grant no. CSIR/09/760(0030)/2017-EMR-I. K.S. used computational resources of the HPCI system (Oakforest-PACS) provided by Joint Center for Advanced High Performance Computing (JCAHPC) through the HPCI System Project (Project ID: hp210023) and computational resources (in art) of the Yukawa-21 System at Yukawa Institute for Theoretical Physics (YITP), Kyoto University. K.S. was supported by the Japan Society for the Promotion of Science (JSPS) KAKENHI, Grant-in-Aid for Early-Career Scientists via grant no. 19K14704. The authors are grateful to the Pelletron staff of IUAC for excellent operation of the accelerator during the experiment and the Target Laboratory personnel of IUAC for fabrication of target foils. Discussions with Dr. Md. Moin Shaikh are thankfully acknowledged.

## References

- [1] Richard Kaufmann and Richard Wolfgang, Nucleon transfer reactions in grazing collisions of heavy ions, *Phys. Rev.* **121**, 192 (1961).
- [2] V. V. Volkov, Deep inelastic transfer reactions –The new type of reactions between complex nuclei, *Phys. Rep.* **44**, 93 (1978).
- [3] G. G. Adamian, N. V. Antonenko, A. Diaz-Torres and S. Heinz, How to extend the chart of nuclides?, *Eur. Phys. J. A* **56**, 47 (2020).
- [4] V. Zagrebaev, W. Greiner, Production of new heavy isotopes in low-energy multinucleon transfer reactions. *Phys. Rev. Lett.* **101**, 122701 (2008).
- [5] G. G. Adamian, N. V. Antonenko, V. V. Sargsyan, W. Scheid, Predicted yields of new neutron rich isotopes of nuclei with  $Z = 64 - 80$  in the multinucleon transfer reaction  $^{48}\text{Ca}+^{238}\text{U}$ , *Phys. Rev. C* **81**, 057602 (2010).
- [6] C. R. Morton, M. Dasgupta, D. J. Hinde, J. R. Leigh, R. C. Lemmon, J. P. Lestone, J. C. Mein, J. O. Newton, H. Timmers, N. Rowley and A. T. Kruppa, Clear signatures of specific inelastic and transfer channels in the distribution of fusion barriers, *Phys. Rev. Lett.* **72**, 4074 (1994).

- [7] G. Pollarolo, Quasielastic Barrier Distributions: Role of Particle Transfer Channels, *Phys. Rev. Lett.* **100**, 252701 (2008).
- [8] K. E. Rehm, Quasi-elastic heavy-ion collisions, *Annu. Rev. Nucl. Part. Sci.* **41**, 429 (1991).
- [9] H. A. Enge, Magnetic spectrographs for nuclear reaction studies, *Nucl. Instrum. Methods* **162**, 161 (1979).
- [10] F. Cappuzzello, C. Agodi, D. Carbone, and M. Cavallaroi, The MAGNEX spectrometer: Results and perspectives, *Eur. Phys. J. A* **52**, 167 (2016).
- [11] M. Rejmund, B. Lecornu, A. Navin, C. Schmitt, S. Damoy, O. Delaune, J. M. Enguerrand, G. Fremont, P. Gangnant, L. Gaudefoy, B. Jacquot, J. Pancin, S. Pullanhiotan, and C. Spitaels, Performance of the improved larger acceptance spectrometer: VAMOS++, *Nucl. Instrum. Methods Phys. Res., Sect. A* **646**, 184 (2011).
- [12] A. Latina, A. M. Stefanini, S. Beghini, B. R. Behera, L. Corradi, G. De Angelis, A. De Rosa, E. Fioretto, A. Gadea, M. Gulmini, G. Inghima, M. LaCommara, G. Maron, R. Menegazzo, N. Marginean, G. Montagnoli, D. R. Napoli, D. Pierroutsakou, G. Pollarolo, M. Romoli, M. Sandoli, F. Scarlassara, S. Szilner, N. Toniolo, M. Trotta, and Y. W. Wu, PRISMA – a magnetic spectrometer for heavy ions at LNL, *Nucl. Phys. A* **734**, E1 (2004).
- [13] J. L. Ferreira, D. Carbone, M. Cavallaro, N. N. Deshmukh, C. Agodi, G. A. Brischetto, S. Calabrese, F. Cappuzzello, E. N. Cardozo, I. Ciraldo, M. Cutuli, M. Fisichella, A. Foti, L. La Fauci, O. Sgouros, V. Soukeras, A. Spatafora, D. Torresi and J. Lubian, Analysis of two-proton transfer in the  $^{40}\text{Ca}(^{18}\text{O}, ^{20}\text{Ne})^{38}\text{Ar}$  reaction at 270 MeV incident energy, *Phys. Rev. C* **103**, 054604 (2021).
- [14] Y. X. Watanabe, Y. H. Kim, S. C. Jeong, Y. Hirayama, N. Imai, H. Ishiyama, H. S. Jung, H. Miyatake, S. Choi, J. S. Song, E. Clement, G. de France, A. Navin, M. Rejmund, C. Schmitt, G. Pollarolo, L. Corradi, E. Fioretto, D. Montanari, M. Niikura, D. Suzuki, H. Nishibata and J. Takatsu, Pathway for the production of neutron-rich isotopes around the  $N = 126$  shell closure, *Phys. Rev. Lett.* **115**, 172503 (2015).
- [15] F. Galtarossa, L. Corradi, S. Szilner, E. Fioretto, G. Pollarolo, T. Mijatović, D. Montanari, D. Ackermann, D. Bourgin, S. Courtin, G. Fruet, A. Goasduff, J. Grebosz, F. Haas, D. Jelavić Malenica, S. C. Jeong, H. M. Jia, P. R. John, D. Mengoni, M. Milin, G. Montagnoli, F. Scarlassara, N. Skukan, N. Soić, A. M. Stefanini, E. Strano, V. Tokić, C. A. Ur, J. J. Valiente-Dobón and Y. X. Watanabe, Mass correlation between light and heavy reaction products in multinucleon transfer  $^{197}\text{Au}+^{130}\text{Te}$  collisions, *Phys. Rev. C* **97**, 054606 (2018).
- [16] I. Stefan, B. Fornal, S. Leoni, F. Azaiez, C. Portail, J. C. Thomas, A. V. Karpov, D. Ackermann, P. Bednarczyk, Y. Blumenfeld, S. Calinescu, A. Chbihi, M. Ciemala, N. Cieplicka-Oryńczak, F.C.L. Crespi, S. Franchoo, F. Hammache, L. W. Iskra, B. Jacquot, R. V. F. Janssens, O. Kamalou, T. Lauritsen, M. Lewitowicz, L. Olivier, S. M. Lukyanov, M. McCormick, A. Maj, P. Marini, I. Matea, M. A. Naumenko, F. de Oliveira Santos, C. Petrone, Yu. E. Penionzhkevich, F. Rotaru, H. Savajols, O. Sorlin, M. Stanoiu, B. Szpak, O. B. Tarasov and D. Verney, Neutron-rich nuclei produced at zero degrees in damped collisions induced by a beam of  $^{18}\text{O}$  on a  $^{238}\text{U}$  target, *Phys. Lett. B* **779**, 456 (2018).
- [17] A. Di Nitto, J. Khuyagbaatar, D. Ackermann, L.-L. Andersson, E. Badura, M. Block, H. Brand, I. Conrad, D.M. Cox, Ch.E. Düllmann, J. Dvorak, K. Eberhardt, P.A. Ellison, N.E. Esker, J. Even, C. Fahlander, U. Forsberg, J.M. Gates, P. Golubev, O. Gothe, K.E. Gregorich, W. Hartmann, R.D. Herzberg, F.P. Heßberger, J. Hoffmann, R. Hollinger, A. Hübner, E. Jäger, B. Kindler, S. Klein, I. Kojouharov, J.V. Kratz, J. Krier, N. Kurz, S. Lahiri, B. Lommel, M. Maiti, R. Mändl, E. Merchán, S. Minami, A.K. Mistry, C. Mokry, H. Nitsche, J.P. Omtvedt, G.K. Pang, D. Renisch, D. Rudolph, J. Runke, L.G. Sarmiento, M. Schädel, H. Schaffner, B. Schausten, A. Semchenkov, J. Steiner, P. Thörle-Pospiech, N. Trautmann, A. Türler, J. Uusitalo, D. Ward, M. Wegrzecki, P. Wiczorek, N. Wiehl, A. Yakushev and V. Yakusheva, Study of non-fusion products in the  $^{50}\text{Ti}+^{249}\text{Cf}$  reaction, *Phys. Lett. B* **784**, 199 (2018).
- [18] H. M. Devaraja, S. Heinz, D. Ackermann, T. Göbel, F. P. Heßberger, S. Hofmann, J. Maurer, G. Münzenberg, A. G. Popeko and A. V. Yeremin, New studies and a short review of heavy neutron-rich transfer products, *Eur. Phys. J. A* **56**, 224 (2020).
- [19] A. K. Azhibekov, V. A. Zernyshkin, V. A. Maslov, Yu. E. Penionzhkevich, K. Mendibayev, T. Issatayev, M. A. Naumenko, N. K. Skobelev, S. S. Stukalov and D. Aznabaev, Differential production cross sections for isotopes of light nuclei in the  $^{18}\text{O}+^{181}\text{Ta}$  reaction, *Phys. Atom. Nucl.* **83**, 93 (2020).
- [20] L. Corradi, G. Pollarolo, and S. Szilner, Multinucleon transfer processes in heavy-ion reactions, *J. Phys. G: Nucl. Part. Phys.* **36**, 113101 (2009).
- [21] R. R. Betts, P. M. Evans, C. N. Pass, N. Poffé, A. E. Smith, L. Stuttgé, J. S. Lilley, D. W. Banes, K. A. Connell, J. Simpson, J. R. H. Smith, A. N. James, and B. R. Fulton, Measurement of sub-barrier transfer reactions for  $^{58}\text{Ni}+\text{Sn}$  using a recoil mass separator, *Phys. Rev. Lett.* **59**, 978 (1987).
- [22] C. N. Pass, P. M. Evans, A. E. Smith, L. Stuttgé, R. R. Betts, J. S. Lilley, D. W. Banes, K. A. Connell, J. Simpson, J. R. Smith, A. N. James, and B. R. Fulton, Study of neutron transfer reactions at sub-Coulomb energies using a recoil separator, *Nucl. Phys. A* **499**, 173 (1989).
- [23] A. N. James, T. P. Morrison, K. L. Ying, K. A. Connell, H. G. Price, and J. Simpson, Microsecond mass separation of heavy compound nucleus residues using the Daresbury recoil separator, *Nucl. Instrum. Methods Phys. Res., Sect. A* **267**, 144 (1988).
- [24] M. G. Herman, L. L. Lee Jr., R. J. Vojtech, S. B. Gazes, M. Satteson, and J. Boyle, Measurements of  $180^\circ$  sub-barrier transfer reaction cross sections in S+Mo,Nb systems, Pages 137-142, *Proc. Symp. Heavy Ion Interactions around the Coulomb Barrier*, Legnaro, Italy, ed. C. Signorini *et al.* (1988); *Lecture Notes in Physics*, Vol. 317. Berlin, Heidelberg: Springer-Verlag (1988).
- [25] R. B. Roberts, S. B. Gazes, J. E. Mason, M. Satteson, S. G. Teichmann, L. L. Lee, Jr., J. F. Liang, J. C. Mahon, and R. J. Vojtech, Sub-barrier one- and two-neutron pickup measurements in  $^{32}\text{S}+^{93}\text{Nb}$ ,  $^{98,100}\text{Mo}$  reactions at  $180^\circ$ , *Phys. Rev. C* **47**, R1831 (1993).
- [26] D. R. Napoli, A. M. Stefanini, H. Moreno Gonzalez, B. Million, G. Prete, P. Spolaore, M. Narayanasamy, Zi Chang Li, S. Beghini, G. Montagnoli, F. Scarlassara, G. F. Segato, C. Signorini, F. Soramel, G. Pollarolo, and A. Rapisarda, Sub-barrier transfer reactions of  $^{32}\text{S}+^{64}\text{Ni}$ , *Nucl. Phys. A* **559**, 443 (1993).
- [27] A. K. Sinha, N. Madhavan, J. J. Das, P. Sugathan, D. O. Kataria, A. P. Patro and G. K. Mehta, Heavy ion reaction analyzer (HIRA): a recoil mass separator facility at NSC, *Nucl. Instrum. Methods Phys. Res., Sect. A* **339**, 543 (1994).
- [28] D. O. Kataria, A. K. Sinha, J. J. Das, N. Madhavan, P. Sugathan, Lagy T. Baby, I. Mazumdar, R. Singh, C. V. K. Baba, Y. K. Agarwal, A. M. Vinodkumar, and K. M. Varier, One- and two-nucleon transfer in the  $^{28}\text{Si}+^{68}\text{Zn}$  system at energies below the Coulomb barrier, *Phys. Rev. C* **56**, 1902 (1997).
- [29] Vandana Tripathi, Lagy T. Baby, P. V. Madhusudhana Rao, S. K. Hui, R. Singh, J. J. Das, P. Sugathan, N. Madhavan, and A. K. Sinha, Measurement of the ground state 2n pickup probability for  $^{28}\text{Si}+^{68}\text{Zn}$  and its role in sub-barrier fusion enhancement, *Pramana – J. Phys.* **53**, 535 (1999).
- [30] Lagy T. Baby, Vandana Tripathi, D. O. Kataria, J. J. Das, P. Sugathan, N. Madhavan, A. K. Sinha, M. C. Radhakrishna, N. M. Badiger, N. G. Puttaswamy, A. M. Vinodkumar, and N. V. S. V. Prasad, Transfer and higher-order phonon coupling effects in the sub-barrier fusion of  $^{28}\text{Si}$  and  $^{93}\text{Nb}$ , *Phys. Rev. C* **56**, 1936 (1997).
- [31] A. K. Sinha in collaboration with L. T. Baby, N. Badiger, J. J. Das, S. K. Hui, D. O. Kataria, R. G. Kulkarni, N. Madhavan, P. V. Madhusudhana Rao, I. Majumdar, M. C. Radhakrishna, N. V. S. V. Prasad, N. G. Puttaswamy, P. Shakeeb, R. Singh, D. L. Shastri, P. Sugathan, V. Tripathi, K. M. Varier, and A. M. Vinodkumar, Sub-barrier few-nucleon transfer reaction and channel coupling effects in heavy ion fusion, *J. Phys. G: Nucl.*

- Part. Phys. **23**, 1331 (1997).
- [32] K. M. Variier, A. M. Vinodkumar, N. V. S. V. Prasad, P. V. Madhusudhana Rao, D. L. Sastry, Lagy T. Baby, M. C. Radhakrishna, N. G. Puttaswamy, J. J. Das, P. Sugathan, N. Madhavan, A. K. Sinha and D. O. Kataria, Transfer measurements for the Ti + Ni systems at near barrier energies, *Pramana – J. Phys.* **53**, 529 (1999).
- [33] Sunil Kalkal, S. Mandal, N. Madhavan, A. Jhingan, E. Prasad, Rohit Sandal, S. Nath, J. Gehlot, Ritika Garg, Gayatri Mohanto, Mansi Saxena, Savi Goyal, S. Verma, B. R. Behera, Suresh Kumar, U. D. Pramanik, A. K. Sinha, and R. Singh, Multinucleon transfer reactions for the  $^{28}\text{Si}+^{90,94}\text{Zr}$  systems in the region below and near the Coulomb barrier, *Phys. Rev. C* **83**, 054607 (2011).
- [34] S. Nath, A Monte Carlo code to calculate transmission efficiency of HIRA, *Nucl. Instrum. Methods Phys. Res., Sect. A* **576**, 403 (2007).
- [35] Rohan Biswas and S. Nath, Simulation of a recoil mass spectrometer for measurement of differential quasi-elastic scattering cross sections, *Eur. Phys. Jour. A* **56**, 1 (2020).
- [36] Rohan Biswas, Sunil Kalkal and S. Nath, Studying multinucleon transfer reaction in a recoil mass spectrometer, *Eur. Phys. J A* **57**, 9 (2021).
- [37] Rohan Biswas, Abhilash S.R., Himanshi Gupta, G.R. Umapathy, Anit Dawar, S. Nath, Fabrication of thin  $^{140,142}\text{Ce}$  target foils for study of nuclear reaction dynamics, *Vacuum* **188**, 110159 (2021).
- [38] <http://www.fresco.org.uk/>
- [39] Ian J. Thompson, Coupled reaction channels calculations in nuclear physics, *Comput. Phys. Rep.* **7**, 167 (1988).
- [40] B. Pritychenko, M. Birch, B. Singh, M. Horoi, Tables of E2 transition probabilities from the first  $2^+$  states in even-even nuclei, *At. Data Nucl. Data Tables* **107**, 1 (2016).
- [41] Ö. Akyüz and A. Winther, Proceedings of the International School of Physics “Enrico Fermi”, Course LXXVII edited by R. A. Broglia, C. H. Dasso, and R. Ricci (North-Holland, Amsterdam, 1981).
- [42] M. Leuschner, J. R. Calarco, F. W. Hersman, E. Jans, G. J. Kramer, L. Lapikás, G. van der Steenhoven, P. K. A. de Witt Huberts, H. P. Blok, N. Kalantar-Nayestanaki and J. Friedrich, Quasielastic proton knockout from  $^{16}\text{O}$ , *Phys. Rev. C* **49**, 955 (1994).
- [43] A. J. Koning and J. P. Delaroche, Local and global nucleon optical models from 1 keV TO 200 MeV, *Nucl. Phys. A* **713**, 231 (2003).
- [44] P. P. Tung, K. A. Erb, M. W. Sachs, G. B. Sherwood, R. J. Ascujtto, and D. A. Bromley, Sequential amplitudes in heavy-ion induced two-proton transfer reactions, *Phys. Rev. C* **18**, 1663 (1978).
- [45] V. Jha, B. J. Roy, A. Chatterjee, H. S. Patel, B. Srinivasan, M. G. Betigeri and H. Machner,  $^{16}\text{O}$ -induced transfer reactions on  $^{90}\text{Zr}$ , *Eur. Phys. J. A* **15**, 389 (2002).
- [46] G. R. Satchler, *Direct Nuclear Reactions* (Oxford University Press, Oxford, 1983).
- [47] Marcos Moshinsky, Transformation brackets for harmonic oscillator functions, *Nucl. Phys.* **13**, 104 (1959).
- [48] K. Sekizawa, Time-Dependent Hartree-Fock Theory and Its Extensions for the Multinucleon Transfer Reactions: A Mini Review, *Front. Phys.* **7**, 20 (2019).
- [49] E. Williams, K. Sekizawa, D. J. Hinde, C. Simenel, M. Dasgupta, I. P. Carter, K. J. Cook, D. Y. Jeung, S. D. McNeil, C. S. Palshetkar, D. C. Rafferty, K. Ramachandran, and A. Wakhle, Exploring Zeptosecond Quantum Equilibration Dynamics: From Deep-Inelastic to Fusion-Fission Outcomes in  $^{58}\text{Ni}+^{60}\text{Ni}$  Reactions, *Phys. Rev. Lett.* **120**, 022501 (2018).
- [50] K. Sekizawa and K. Hagino, Time-dependent Hartree-Fock plus Langevin approach for hot fusion reactions to synthesize the  $Z = 120$  superheavy element, *Phys. Rev. C* **99**, 051602(R) (2019).
- [51] K. Sekizawa and S. Ayik, Quantal diffusion approach for multinucleon transfer processes in the  $^{58,64}\text{Ni}+^{208}\text{Pb}$  reactions: Toward the production of unknown neutron-rich nuclei, *Phys. Rev. C* **102**, 014620 (2020).
- [52] S. Ayik and K. Sekizawa, Kinetic energy dissipation and fluctuations in strongly-damped heavy-ion collisions within the stochastic mean-field approach, *Phys. Rev. C* **102**, 064619 (2020).
- [53] C. Simenel and A. S. Umar, Heavy-ion collisions and fission dynamics with the time-dependent Hartree-Fock theory and its extensions, *Prog. Part. Nucl. Phys.* **103**, 19 (2018).
- [54] P. D. Stevenson and M. C. Barton, Low-energy heavy-ion reactions and the Skyrme effective interaction, *Prog. Part. Nucl. Phys.* **104**, 142 (2019).
- [55] K. -H. Kim, T. Otsuka, and P. Bonche, Three-dimensional TDHF calculations for reactions of unstable nuclei, *J. Phys. G: Nucl. Part. Phys.* **23**, 1267 (1997).
- [56] E. Chabanat, P. Bonche, P. Haensel, J. Meyer, and R. Schaeffer, New Skyrme Effective Forces for Supernovae and Neutron Rich Nuclei, *Phys. Scr.* **T56**, 231 (1995).
- [57] C. Simenel, Particle Transfer Reactions with the Time-Dependent Hartree-Fock Theory Using a Particle Number Projection Technique, *Phys. Rev. Lett.* **105**, 192701 (2010).
- [58] S. Ebata, T. Nakatsukasa, T. Inakura, K. Yoshida, Y. Hashimoto, and K. Yabana, Canonical-basis time-dependent Hartree-Fock-Bogoliubov theory and linear-response calculations, *Phys. Rev. C* **82**, 034306 (2010).
- [59] G. Scamps and D. Lacroix, Effect of pairing on one- and two-nucleon transfer below the Coulomb barrier: a time-dependent microscopic description, *Phys Rev C* **87**, 014605 (2013).
- [60] P. Magierski, K. Sekizawa, and G. Wlazlowski, Novel role of superfluidity in low-energy nuclear reactions, *Phys Rev Lett.* **119**, 042501 (2017).
- [61] Y. Hashimoto and G. Scamps, Gauge angle dependence in time-dependent Hartree-Fock-Bogoliubov calculations of  $^{20}\text{O}+^{20}\text{O}$  head-on collisions with the Gogny interaction, *Phys Rev C* **94**, 014610 (2016).
- [62] G. Scamps and Y. Hashimoto, Transfer probabilities for the reactions  $^{14,20}\text{O}+^{20}\text{O}$  in terms of multiple time-dependent Hartree-Fock-Bogoliubov trajectories, *Phys Rev C* **96**, 031602(R) (2017).
- [63] D. Regnier, D. Lacroix, G. Scamps, and Y. Hashimoto, Microscopic description of pair transfer between two superfluid Fermi systems: Combining phase-space averaging and combinatorial techniques, *Phys. Rev. C* **97**, 034627 (2018).
- [64] M. Cavallaro, F. Cappuzzello, M. Bondi, D. Carbone, V. N. Garcia, A. Gargano, S. M. Lenzi, J. Lubian, C. Agodi, F. Azaiez, M. De Napoli, A. Foti, S. Franchoo, R. Linares, D. Nicolosi, M. Niikura, A. Scarpaci and S. Tropea, Quantitative analysis of two-neutron correlations in the  $^{12}\text{C}(^{18}\text{O}, ^{16}\text{O})^{14}\text{C}$  reaction, *Phys. Rev. C* **88**, 054601 (2013).